ELSEVIER

Thermochimica Acta 377 (2001) 183–191

thermochimica acta

www.elsevier.com/locate/tca

Thermal conductivity from dynamic response of DSC

M. Merzlyakov*, C. Schick

Department of Physics, University of Rostock, Universitätsplatz 3, D-18051 Rostock, Germany

Received 28 February 2001; received in revised form 25 March 2001; accepted 28 March 2001

Abstract

We proposed a method to measure the absolute value of thermal conductivity κ of low thermal conducting solid materials (with κ in the range 0.1–2 W m^{-1} K^{-1}). The accuracy of thermal conductivity determination is typically better than 10%. Thermal conductivity and heat capacity of the sample are determined simultaneously in a single measurement with the prerequisite that these values are frequency independent. Technically this method is realized on power-compensated differential scanning calorimeters (DSCs) without any modification in the measuring system. DSC is calibrated in a standard way for temperature and heat flow. No special calibration for thermal conductivity is necessary. The method uses temperature–time profiles consisting of one fast temperature jump of 0.5–2 K and an isotherm. The measuring time for each temperature is less than 1 min. As input parameters only sample thickness and contact area with the DSC furnace (or sample diameter if the sample is disk shaped) are needed together with sample mass. In addition to the sample thermal conductivity and heat capacity, the effective thermal contact between sample and DSC furnace is determined. Data evaluation is performed automatically by a program available for download.

Keywords: Thermal conductivity; Heat capacity; Thermal diffusivity; DSC; Polymers

1. Introduction

Thermal conductivity data are in great demand by industry, for use in polymer injection molding, in encapsulation of electronic devices and, in general, in modeling of different processes. Nowadays commercial techniques often measure thermal diffusivity or effusivity and calculate thermal conductivity using heat capacity values, measured separately.

Differential scanning calorimeter (DSC) is a commercially available and widely used technique to measure heat capacity of samples of milligram size in a wide temperature range. Therefore, it would be opportune to add to DSC instruments a feature to measure thermal conductivity of typical DSC samples.

As reported first by Marcus and Blaine [1], thermal conductivity can be measured without modification of the commercially available DSC cell. They calculate thermal conductivity from the ratio of apparent and true heat capacities measured for a thick (about 3 mm) and a thin (about 0.5 mm) sample, respectively, in temperature modulated mode. They use one additional calibration step to take into account heat losses through the purge gas surrounding. The method is based on the assumption that ''the face of the specimen at the heat source follows the applied temperature modulation'' [1], which means no thermal resistance between the sample and the furnace.

Simon and McKenna [2] show two problems in the method proposed by Marcus and Blaine. First, the equation relating the apparent heat capacity to the

* Corresponding author. Tel.: +49-381-498-1616; fax: +49-381-498-1626.
E-mail address: mikhail.merzliakov@physik.uni-rostock.de (M. Merzlyakov).

0040-6031/01/$ – see front matter
PII: S0040-6031(01)00553-6

Nomenclature

c_p	specific heat capacity of the sample
d	sample effective thickness (half of the actual thickness for a sample sealed in a pan)
K_{op}	thermal contact between furnace and pan
K_{ps}	thermal contact between pan and sample
S	contact area
$T_o(t)$	furnace temperature
$T_p(t)$	pan temperature
$T_s(x,t)$	sample temperature
Greek letters	
κ	thermal conductivity of the sample
ρ	sample density
$\Phi_o(t)$	heat flow rate into the pan–sample system
$\Phi_p(t)$	heat flow rate into the sample

thermal conductivity is limited in range due to an approximation made in their derivation ([3]). Second, a thermal resistance between the sample and the furnace can have a significant effect on the measured apparent heat capacity. They, as well as Marcus and Reading [4], also mention that thermal conductivity could be easily obtained from a single sample run at several frequencies, i.e. it is not necessary to measure two samples. But what is necessary in any case is to know the heat transfer coefficient. ''If the heat transfer coefficient is not known, an accurate value of thermal conductivity cannot be obtained'' [2].

We based our method on the model presented in [5]. With this model, one can thoroughly describe the dynamic behavior of DSC and temperature modulated DSC (TMDSC) systems under conditions of an appreciable temperature gradient inside the sample. The question arises how to get all the parameters of the model. Below, on the example of one measurement, we present an algorithm to determine the most important parameters: sample heat capacity, effective thermal contact between the sample and the furnace and finally sample thermal conductivity for the case of real valued heat capacity and thermal conductivity. Further, we present experimental results with different solid samples and various experimental conditions. Measured thermal conductivity data are compared with expected values. Finally, we discuss possible reasons for some systematic bias between measured and expected thermal conductivity values. We analyze the validity of used model and how it can be monitored by measured results. We make some suggestions how to improve the method.

2. Data treatment

2.1. The idea

The idea is the following: how good temperature waves propagate through the sample under investigation is measured in the DSC apparatus. Low frequency temperature waves go through the whole sample without damping, the whole sample is modulated and therefore, a large apparent heat capacity is measured. Higher frequency temperature waves are damped and the sample is partly modulated — the measured apparent heat capacity is smaller. The damping is stronger for poor thermal conducting materials. This is basically also the idea of the methods proposed by Marcus and Blaine [1] and Simon and McKenna [2]. However, the same damping effect appears by finite thermal contact (heat transfer coefficient) between sample surface and the furnace — a poor thermal contact damps the temperature waves stronger than a good one. But the thermal contact and thermal conductivity lead to different frequency dependencies of apparent heat capacity [5]. This difference allows the necessary separating of damping effects due to the thermal contact and due to the thermal conductivity. This approach overcomes the limitations discussed by Simon and McKenna [2]. Moreover, it is not necessary to measure apparent heat capacity at different frequencies with TMDSC. The spectrum of temperature waves can be easily generated by a single step in the program temperature [6].

2.2. The algorithm

The DSC set-up, described in [5], is simplified to the case when a solid sample is measured directly in the DSC furnace, see Fig. 1 and Appendix A. Three parameters need to be determined: specific heat capacity c_p, effective thermal contact between the sample and the furnace K and thermal conductivity κ.

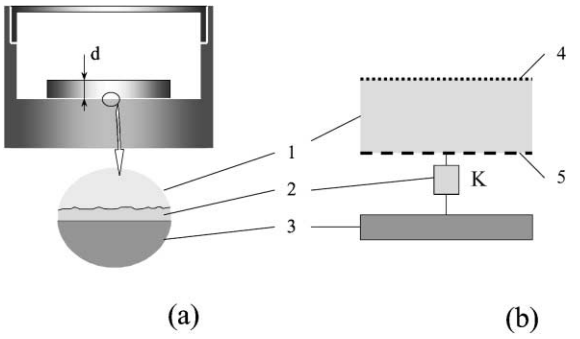

Fig. 1. The schematic view of the furnace (a) and its block diagram (b). 1 – sample, 2 – grease layer, which produces an effective thermal contact K, 3 – DSC furnace, 4 – adiabatic layer at upper surface of the sample, 5 – bottom surface of the sample.

Effective heat capacity $C_{\mathrm{eff}}(\omega)$ at different frequencies can be calculated from step response analysis [6] as a ratio of heat flow rate amplitude A_{HF} and heating rate amplitude A_q:

$$C_{\mathrm{eff}}(\omega) = \frac{A_{\mathrm{HF}}}{A_q} = \frac{\sum_{i=1}^{n} \mathrm{HF}_i \cos(\omega t_i) - \mathrm{i}\sum_{i=1}^{n} \mathrm{HF}_i \sin(\omega t_i)}{\sum_{i=1}^{n} q_i \cos(\omega t_i) - \mathrm{i}\sum_{i=1}^{n} q_i \sin(\omega t_i)} \quad (1)$$

where points of heat flow rate, HF_i, and heating rate, q_i, should be taken both with the same sampling rate (number of points per unit time). We collect the points from the beginning of the temperature step until the heat flow reaches the steady state value at the isotherm [6], having in total n points. After that the $C_{\mathrm{eff}}(\omega)$ values should be corrected for apparatus influence (instrumental delay) [5,7] as

$$C_{\mathrm{app}}(\omega) = C_{\mathrm{eff}}(\omega) B_2(\omega) \quad (2)$$

where $C_{\mathrm{app}}(\omega)$ is an apparent heat capacity at frequency ω, $B_2(\omega)$ is the dynamic calibration factor of the instrument [5,7].

The first parameter of the system, the specific heat capacity c_{p}, can be easily determined as

$$c_{\mathrm{p}} = \frac{C_{\mathrm{eff}}(0)}{m_{\mathrm{s}}} \quad (3)$$

where m_{s} is the sample mass and $C_{\mathrm{eff}}(0)$ is calculated from Eq. (1) for $\omega = 0$.

The two other parameters are determined as described below.

As an example, we took the apparent heat capacity data of a poly(ε-caprolactone) (PCL) disk with thickness $d = 1.42$ mm and diameter of about 6 mm. From Eq. (A.4), in Appendix A, it follows that apparent heat capacity is given as

$$C_{\mathrm{app}}(\omega) = \frac{C_\alpha(\omega)}{1 - (\mathrm{i}\omega/K) C_\alpha(\omega)} \quad (4)$$

where $C_\alpha(\omega)$ is the apparent heat capacity in case of ideal thermal contact between the sample and the furnace. In other words, it is the apparent heat capacity one would measure directly on the bottom surface of the sample (Fig. 1). We rewrite Eq. (4) as

$$C_\alpha(\omega) = \frac{C_{\mathrm{app}}(\omega)}{1 + (\mathrm{i}\omega/K) C_{\mathrm{app}}(\omega)} \quad (5)$$

Unknown parameter in Eq. (5) is K because $C_{\mathrm{app}}(\omega)$ is measured. Values of $C_{\mathrm{app}}(\omega_k)$ for a set of different frequencies ω_k and $C_\alpha(\omega_k)$ for three different values of K are shown on Fig. 2. The lower the frequency ω_k the larger the modulus of $C_{\mathrm{app}}(\omega_k)$ and $C_\alpha(\omega_k)$.

On the other hand, $C_\alpha(\omega)$ should be described by Eq. (A.3) (see Appendix A), solid curve in Fig. 2. The theoretical $C_\alpha(\omega)$ curve in a polar plot representation depends only on the value $C_\alpha(\omega = 0)$, that is sample true heat capacity $c_{\mathrm{p}} m_{\mathrm{s}}$, and does not depend on all other parameters. The correct value for K is then the value at which all $C_\alpha(\omega_k)$ points, calculated by Eq. (5), lie on the theoretical curve. In this case, $K = 0.029\ \mathrm{W\ K^{-1}}$. In this way, the second parameter of the system has been determined.

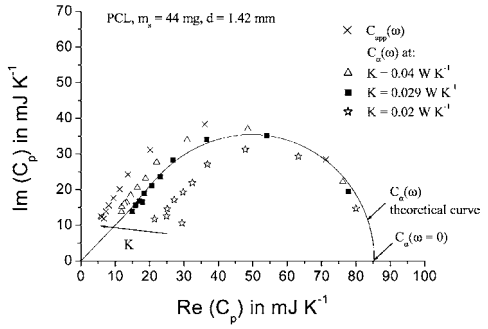

Fig. 2. Polar plot of $C_{\mathrm{app}}(\omega_k)$ and $C_\alpha(\omega_k)$ for effective thermal contact K. The horizontal and vertical axes show the real and imaginary parts, respectively. Solid curve is theoretical values of $C_\alpha(\omega)$ for given $C_\alpha(\omega = 0)$.

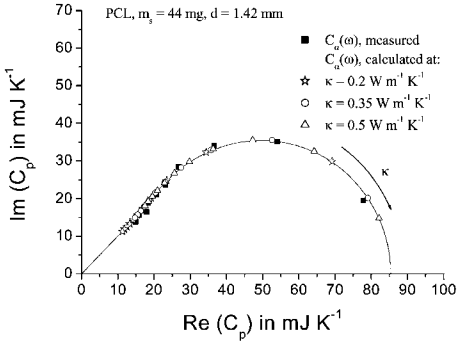

Fig. 3. Polar plot of $C_\alpha(\omega_k)$, measured and calculated for different values of thermal conductivity κ. The horizontal and vertical axes show the real and imaginary parts, respectively.

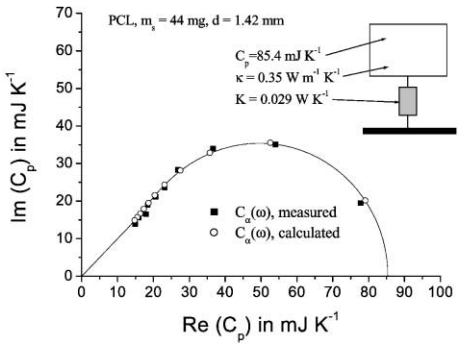

Fig. 4. Polar plot of $C_\alpha(\omega_k)$, calculated with optimal parameter κ and measured. The horizontal and vertical axes show the real and imaginary parts, respectively.

Next step is to determine sample thermal conductivity κ. All parameters in Eq. (A.3) (see Appendix A), except thermal conductivity κ, are known (density ρ can be calculated from the sample mass and sample size, which are set before measurement). At any given frequency $\omega_k \neq 0$ increasing of κ leads to shifting the position of the $C_\alpha(\omega_k)$ point on the theoretical curve towards $C_\alpha(\omega = 0)$ (Fig. 3).

By varying κ in Eq. (A.3) (see Appendix A), the condition is reached where the same set of ω_k calculated $C_\alpha(\omega_k)$ points coincide with measured points $C_\alpha(\omega_k)$, determined by Eq. (5). In this case, it happens at $\kappa = 0.35$ W m^{-1} K^{-1}. Thus, the third parameter of the system has been determined.

As one can see from Fig. 4, the measured points for $C_\alpha(\omega_k)$ coincide not exactly with theoretical ones, but this scatter corresponds to only 1–2% uncertainties in determination of thermal conductivity κ and effective thermal contact K.

The algorithm to determine thermal conductivity and effective thermal contact from the spectrum of $C_{app}(\omega_k)$ is realized on MS-Excel™ spreadsheet with Visual Basic™ macros.[1]

3. Experimental results

Four samples with known thermal conductivity were measured: polystyrene (PS) and poly(methyl methacrylate) (PMMA) (ASTM interlaboratory test for thermal conductivity by modulated temperature DSC) and epoxy resins 160 and 4173 (provided by Mathis Instruments). Samples were prepared in disk shape with diameter $D = 6$ mm (epoxy resins) and $D = 6.4$ mm (PS and PMMA) and thickness d of about 0.5 and 1 mm. The measurements were performed by Perkin-Elmer Pyris-1 DSC with Lauda RC6 cooling system. DSC block temperature was set to +5°C. Purge gas was nitrogen with gas flow of 20 ml min^{-1}. Since the furnace floor is slightly curved [8] and the disks are not flexible we used Apiezon™ grease to get homogeneous thermal contact over the whole contact area between the bottom of the sample and the furnace. It is more important to homogenize the contact rather then to minimize its resistance. Temperature–time program shown in Fig. 5 was used to generate the spectrum of apparent heat capacity.

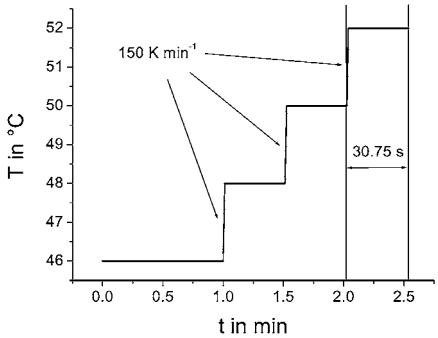

Fig. 5. Temperature–time program, consisting of 2 K steps in temperature and 30 s isotherms. Temperature steps were programmed as short heating segments with 150 K min^{-1} heating rate.

[1] See WWW (Internet) URL: http://www.uni-rostock.de/fakult/manafak/physik/poly/.

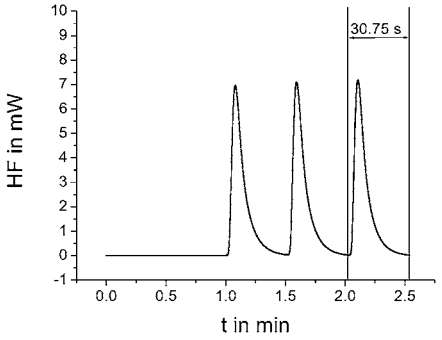

Fig. 6. An example of measured heat flow rate HF vs. time which corresponds to the temperature–time program, shown in Fig. 4. The last peak was taken for further data evaluation.

Initial isotherm of 1 min was added to check whether heat flow drift at steady state is remarkable. Corresponding heat flow rate after empty furnace correction is shown in Fig. 6 (since we did not use a pan, we subtracted the heat flow measured with an empty furnace).

In this example, the last step was evaluated. Interesting point here is that heat flow in the last step did not really start from steady state neither reach steady state at the end but it is still possible to evaluate correctly the data. This fact allows shortening the duration of the measurement, as discussed in [6].

We took into consideration up to seven frequencies $\omega_k = k\omega_0$, $k = \{1, 2, \ldots, 7\}$, $\omega_0 = 2\pi/t_p$ and period $t_p = 30.75$ s. The results of thermal conductivity determination are shown in Table 1.

The measured data are also presented in polar plots (Fig. 7), where measured apparent heat capacity $C_\alpha(\omega_k)$ (filled symbols) is compared with calculated

Table 1
Comparative thermal conductivities measured at 51°C for four different samples

Material	Measured κ (W m^{-1} K^{-1})	Expected κ (W m^{-1} K^{-1})
PS	0.168–0.172	0.1562 [9][a]
PMMA	0.212–0.215	0.197 [10][b]
Epoxy resin 160	0.63	0.61[c]
Epoxy resin 4173	1.70–1.85	1.83[c]

[a] The value is taken at 47°C.
[b] The value is taken at 47.2°C.
[c] The value from hot disk measurements was kindly provided by Mathis Instruments, Canada.

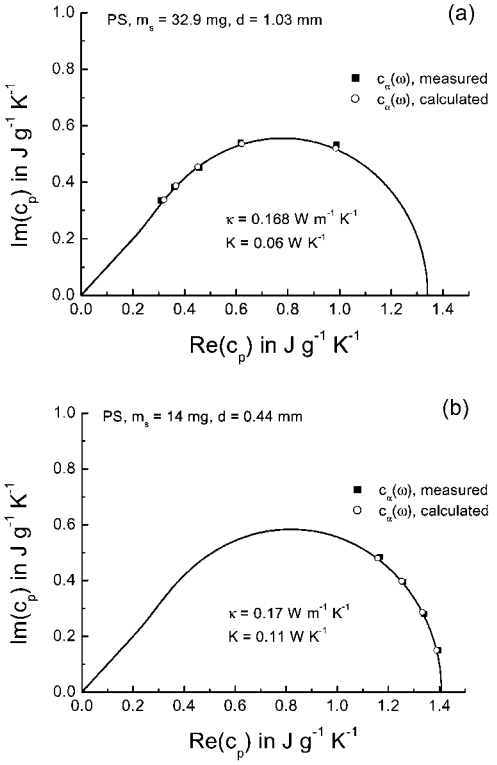

Fig. 7. Polar plot of $C_\alpha(\omega_k)$, measured and calculated, for PS disks with thickness 1.03 mm (a) and 0.44 mm (b). The horizontal and vertical axes show the real and imaginary parts, respectively.

ones (open symbols). We plot specific values for better comparison of the results for different sample masses. Solid line corresponds to theoretical curve of $C_\alpha(\omega)$, see Eq. (A.3) (Appendix A).

As one can see from Fig. 7, the two PS disks with different thickness give quite different values of $C_\alpha(\omega_k)$ at the same set of frequencies. However, both sets of $C_\alpha(\omega_k)$ give almost the same value of thermal conductivity κ of about 0.17 W m^{-1} K^{-1}, that is the property of the material. One comes to the same conclusion with the PMMA results (Fig. 8) — thermal conductivity for thin and thick samples is about 0.214 W m^{-1} K^{-1}.

The effective thermal contact K is not necessarily the same for these measurements, because it depends on the actual positioning of the disk and of the amount of the grease used. In general, the more grease one use the better the thermal contact is (larger value of K). We used relative small amount of grease (in order of

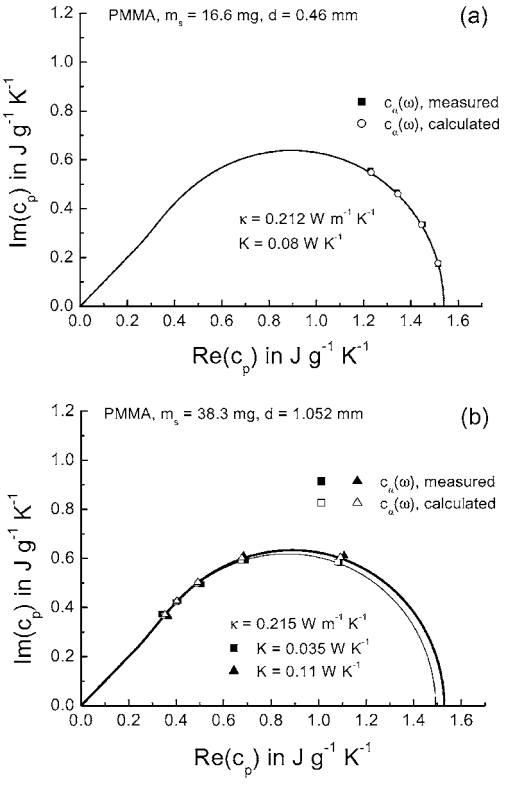

Fig. 8. Polar plot of $C_\alpha(\omega_k)$, measured and calculated, for PMMA disks with thickness 0.46 mm (a) and 1.052 mm (b). The horizontal and vertical axes show the real and imaginary parts, respectively. In part (b) $C_\alpha(\omega_k)$ values are shown for two different effective thermal contacts $K_1 = 0.035$ W K^{-1} and $K_2 = 0.11$ W K^{-1} and slightly different c_p.

0.5–1 mg) that was enough to wet the surface of the disk and the furnace but not necessarily to occupy whole space between them. In Fig. 8b, $C_\alpha(\omega_k)$ values are obtained from two different measurements of the same disk ($d = 1.052$ mm, $D = 6.4$ mm) with different amount of grease. In spite of the large difference in thermal contact ($K_1 = 0.035$ W K^{-1}, $K_2 = 0.11$ W K^{-1}), the same value for thermal conductivity ($\kappa = 0.215$ W m^{-1} K^{-1}) is obtained. Again the model correctly describes the results. It is important to mention that specific heat capacity in these two measurements (thin and thick curves) is different. Additional heat capacity of the grease in second measurement (thick curve) increases total measured heat capacity which is normalized to the same sample mass.

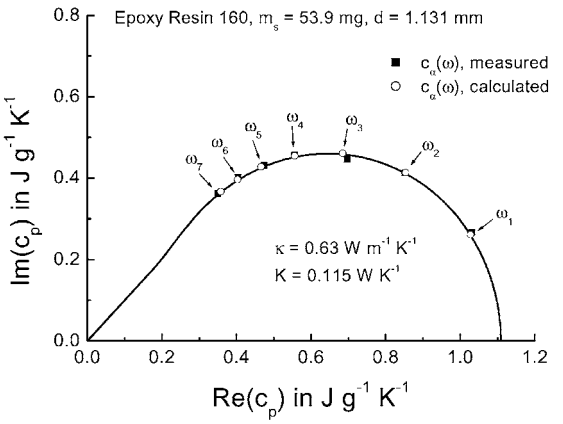

Fig. 9. Polar plot of $C_\alpha(\omega_k)$, measured and calculated, for epoxy resin 160 disk with 1.131 mm thickness. The horizontal and vertical axes show the real and imaginary parts, respectively.

Of course, the measured points coincide with calculated ones only to some extend. There is always some scatter in the data. For example, in the results for epoxy resin 160, measured $C_\alpha(\omega_3 = 3\omega_0)$ deviates relatively strong from calculated value (Fig. 9).

Some difficulties appeared when we measured material with relatively high thermal conductivity (epoxy resin 4173). At the given sample thickness, the temperature waves are damped only slightly and the finite thermal conductivity gives similar frequency dependence of $C_\alpha(\omega)$ as the thermal contact. That is why there are some uncertainties in determination of thermal conductivity (Fig. 10).

Here the same measured dataset can give slightly lower thermal contact K and higher thermal conductivity κ or higher K and lower κ — measured and calculated points in both cases more or less coincide. It is impossible to narrow the range of K and κ to get the correct pair.

In this case, the way to resolve the influences from thermal contact K and thermal conductivity κ is to increase further the frequency of temperature waves (to take much higher number for k in $\omega_k = k\omega_0$, which used in Eq. (1)). But in our measurements $C_\alpha(\omega)$ values were very uncertain at k higher than 7 (Fig. 11).

We also observed for a few measurements some disagreement with the model (Fig. 12). For these measurements, it is impossible to fit simultaneously all calculated $C_\alpha(\omega_k)$ values with the measured ones because we always have some systematic differences.

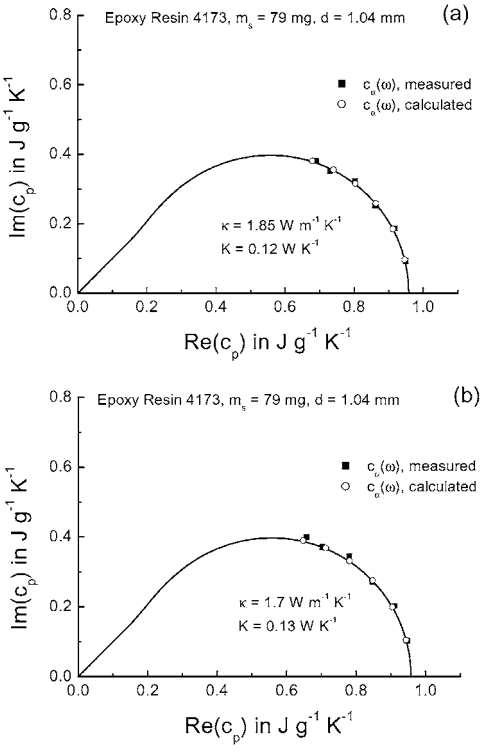

Fig. 10. Polar plot of $C_\alpha(\omega_k)$, measured and calculated, for epoxy resin 4173. The horizontal and vertical axes show the real and imaginary parts, respectively. Two different sets of parameters κ and K ($\kappa = 1.85$ W m^{-1} K^{-1}, $K = 0.12$ W K^{-1} (a) and $\kappa = 1.7$ W m^{-1} K^{-1}, $K = 0.13$ W K^{-1} (b)) describe the measured points with the same quality.

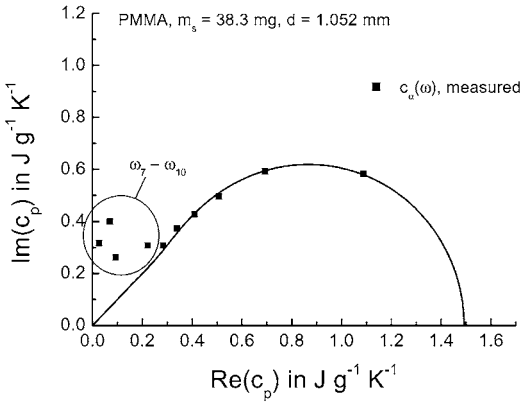

Fig. 11. Polar plot of $C_\alpha(\omega_k)$ for a PMMA disk. The horizontal and vertical axes show the real and imaginary parts, respectively. $C_\alpha(\omega_k)$ values, measured at high frequencies (ω_7 to ω_{10}), are uncertain.

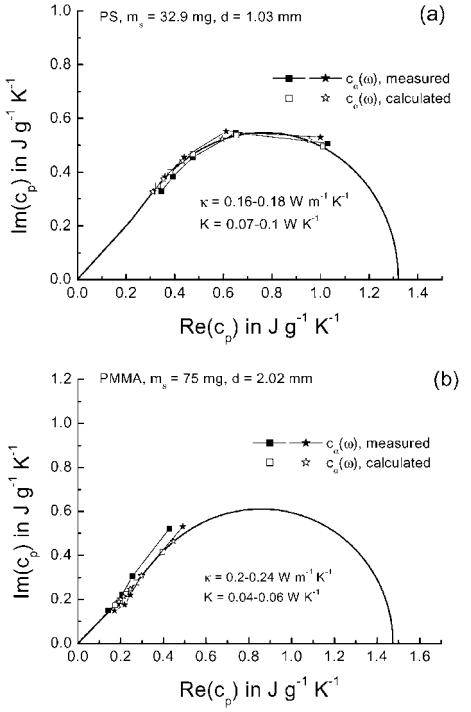

Fig. 12. Polar plot of $C_\alpha(\omega_k)$ for PS (a) and PMMA (b) disks. The horizontal and vertical axes show the real and imaginary parts, respectively. Measured and calculated values do not coincide simultaneously for the whole set of frequencies ω_k.

There could be two reasons for this disagreement: inhomogeneous thermal contact in case of thin disk (Fig. 12a), or too thick disk (Fig. 12b). In both cases, the one-dimensional model used for calculation could not give exact values of thermal conductivity. But one can get some range of possible value of thermal conductivity. From the width of the range one gets an impression about the validity of the model to describe the given experimental conditions, or, put another way, how faulty were the experimental conditions.

4. Discussion

The one-dimensional model we used in the method assumes a negligible heat flow through the upper surface of the sample disk. Certainly it is true only to some extent. There is some heat flow through the purge gas to the sample inside the measuring cup. This

heat flow would shift the adiabatic layer from the upper surface downwards into the sample. This would lead to a shortening of the effective sample thickness d and as a result to overestimated thermal conductivity values, which are calculated for a larger actual thickness. The overestimation of the thermal conductivity values for low thermal conducting samples (PS and PMMA, see Table 1) can be assigned to this reason. This effect is minor for higher thermal conducting materials because the heat flow through the sample is larger.

The one-dimensional model also assumes no radial heat flow inside the sample and a homogeneous thermal contact between the bottom surface of the disk and the furnace. If the model fails to describe the actual more complicated sample set-up (e.g. inhomogeneous thermal contact), the measured $C_\alpha(\omega_k)$ would not agree with the calculated $C_\alpha(\omega_k)$, as shown in Fig. 11. This can be used as an internal test of the validity of the model. By the way, the model is not designed to describe a case of complex frequency-dependent heat capacity. Therefore, for complex heat capacity, the method results in uncertain thermal conductivity values.

As can be seen form Figs. 6 and 7, the model already describes well various experimental data. The same values of thermal conductivity for different sample thickness and effective thermal contacts were obtained.

There are three directions for further improvement of this method of thermal conductivity measurement. First, the heat flow through the purge gas may be considered to improve the accuracy of thermal conductivity determination. Second, the sample pan effect, presented in [5], may be considered. Using a pan will allow measuring liquid samples and samples which undergo liquid-to-solid transitions in a broad temperature range. Third, heat capacity and thermal conductivity may be considered as being complex and frequency-dependent values and measured within transition (like glass transition or melting). However, it would be possible to separate influence of heat transfer (thermal conductivity and thermal contact) and frequency dependence of heat capacity only by performing at least two measurements of two samples with different thickness.

If more precise heat capacity values are desired, one can account for additional heat capacity of the grease in the following way: first, a small amount of the grease is smeared over the clean furnace and an empty furnace run is recorded; then the clean sample is placed on top of the grease layer and the sample run is recorded; after that the furnace is cleaned and the next grease layer is prepared for the next empty furnace run. It is also not necessary to know the exact amount of the grease in the furnace. If the measured sample should be measured once again, first it should be cleaned form the grease from the last measurement.

5. Conclusion

The proposed method permits thermal conductivity and heat capacity of low thermal conducting materials to be determined in a single run using standard power-compensated DSC. Accuracy of thermal conductivity determination is about 10% (Marcus and Blaine reported the precision of their approach of 3% [1], what is questionable [2]). No modifications of the instrument are needed. The whole measurement can take less than 1 min for each temperature of interest. In addition to thermal conductivity and heat capacity, the effective thermal contact between sample and DSC furnace is determined. The method has an internal check of the correctness of the measured results. In case of a faulty measurement, it reports a possible range of thermal conductivity and thermal contact.

Acknowledgements

This work was financially supported by Perkin-Elmer Instruments, USA. The authors are grateful to ASTM Committee E37 on Thermal Measurements, USA, and Mathis Instruments, Canada, for providing the samples.

Appendix A

A schematic representation of the sample–pan–furnace system is shown in Fig. 13 [5].

Solving the heat transfer equation for such a model, where a relatively thin sample can be considered as a one-dimensional system, one can get the following

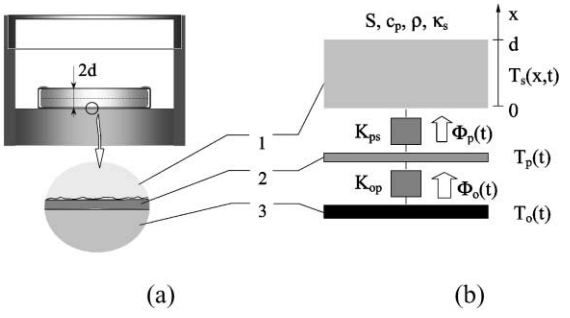

Fig. 13. The schematic view of the furnace (a) and its block diagram (b). 1 − sample, 2 − pan, 3 − DSC furnace.

expression for the apparent heat capacity $C_{app}(\omega)$ of the sample–pan–furnace system:

$$C_{app}(\omega) = \frac{C_p + C_\beta(\omega)}{1 - (i\omega/K_{op})(C_p + C_\beta(\omega))} \quad (A.1)$$

where C_p is the heat capacity of the pan,

$$C_\beta(\omega) = \frac{C_\alpha(\omega)}{1 - (i\omega/K_{ps})C_\alpha(\omega)} \quad (A.2)$$

denotes the apparent heat capacity which would be measured directly at the surface of the sample pan and

$$C_\alpha(\omega) = -\frac{1}{i\omega}\kappa S\alpha \tanh(\alpha d) \quad (A.3)$$

denotes the apparent heat capacity which would be measured directly at the surface of the sample, $\alpha = \sqrt{\omega/|\chi|}\exp\{(i/2)\arg(-i(\omega/\chi))\}$, $\chi = \kappa/\rho c_p$ is the thermal diffusivity [5]. Eqs. (A.1)–(A.3) are complex and valid also for complex frequency-dependent κ and c_p.

For the method of thermal conductivity determination, it is assumed that κ and c_p are real valued and frequency independent. The sample–pan–furnace system may be simplified by excluding the pan. The sample disk is measured directly in the DSC furnace (Fig. 1). In this case, the sample disk is heated only from bottom, therefore, an adiabatic layer is assumed at the upper surface of the disk. Effective sample thickness d is then the actual sample thickness and the contact area S is the bottom surface area of the disk. In Eq. (A.1) setting $C_p = 0$ and $K_{op} \to \infty$ leads to $C_{app}(\omega) = C_\beta(\omega)$. Eq. (A.1) is rewritten as

$$C_{app}(\omega) = \frac{C_\alpha(\omega)}{1 - (i\omega/K)C_\alpha(\omega)} \quad (A.4)$$

where now K is the effective thermal contact between the bottom sample surface and the furnace.

References

[1] S.M. Marcus, R.L. Blaine, Thermochim. Acta 243 (1994) 231–239.
[2] S.L. Simon, G.B. McKenna, J. Reinforced Plastics Composites 18 (1999) 559–571.
[3] R.L. Blaine, S.M. Marcus, J. Thermal Anal. 54 (1998) 467–476.
[4] S.M. Marcus, M. Reading, Method and apparatus for thermal conductivity measurements, US Patent 5,334,994, 8 August 1994.
[5] M. Merzlyakov, C. Schick, Thermochim. Acta 330 (1999) 65–73.
[6] M. Merzlyakov, C. Schick, Thermochim. Acta, submitted.
[7] G.W.H. Höhne, M. Merzlyakov, C. Schick, Thermochim. Acta, in preparation.
[8] S.M. Sarge, W. Poeβnecker, Thermochim. Acta 329 (1999) 17–21.
[9] C.Y. Ho, P.D. Desai, K.T. Wu, T.N. Havill, T.Y. Lee, NBS Publication GCR-77-83, 1977.
[10] D.R. Salmon, National Physical Laboratory, Teddington, Middlesex, TW11 OLW, England, 1993.